Science of the Total Environment 575 (2017) 429–436

Contents lists available at ScienceDirect

Science of the Total Environment

journal homepage: www.elsevier.com/locate/scitotenv

A synchronous observation of enhanced aerosol and NO_2 over Beijing, China, in winter 2015

Zhenyi Chen [a], Cheng Liu [a,b,c,*], Wenqing Liu [a], Tianshu Zhang [a], Jin Xu [a]

[a] Key Lab of Environmental Optics & Technology, Anhui Institute of Optics and Fine Mechanics, Chinese Academy of Sciences, Hefei 230031, China
[b] School of Earth and Space Sciences, University of Science and Technology of China, Hefei 230026, China
[c] CAS Center for Excellence in Regional Atmospheric Environment, Institute of Urban Environment, Chinese Academy of Sciences, Xiamen 361021, China

HIGHLIGHTS

- First simultaneous observations of aerosols and NO_2 in a pollution episode in Beijing was investigated.
- High averaged aerosol extinction was observed and NO_2 showed similar temporal variations with much weaker diurnal evolution.
- The enhancement of NO_2 from satellite data testified the pollution and backward trajectories indicated the possible sources.

GRAPHICAL ABSTRACT

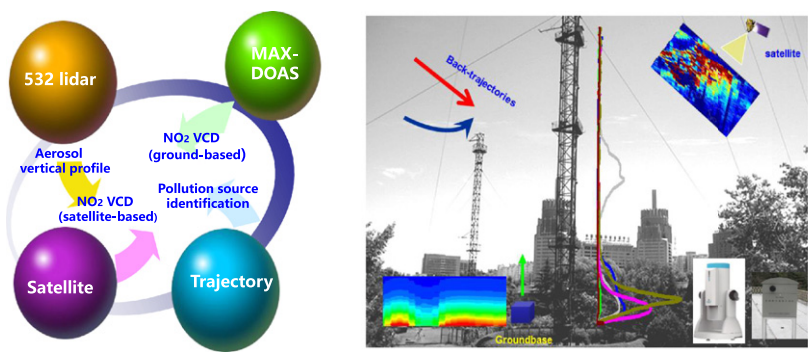

ARTICLE INFO

Article history:
Received 26 April 2016
Received in revised form 23 September 2016
Accepted 23 September 2016
Available online 14 October 2016

Keywords:
Aerosol
NO_2
Lidar
MAX-DOAS

ABSTRACT

Despite extensive efforts into the characterization of air pollution during the past decade, concurrent real-time characterization of aerosol and NO_2 as well as satellite observation above the urban canopy in the megacity of Beijing has sparsely been performed to date. We conducted a simultaneous real-time measurement of aerosol and NO_2 in urban Beijing in a pollution episode from November 25, 2015 to December 2, 2015. The aerosol extinction coefficient was measured by a 532 Mie lidar and the NO_2 concentration by a Multi-Axis Differential Optical Absorption Spectroscopy (MAX-DOAS). The highest aerosol extinction coefficient was 1.55 ($\pm$0.16) km^{-1} at 532 m at a height of 0.27 km. The high average aerosol extinction was observed throughout the pollution period, probably due to the favorable static weather conditions under high surface high-pressure system and transportation sources. NO_2 showed similar temporal variations between ground level and 0.3 km, whereas a much weaker diurnal evolution was found for NO_2. The boundary layer structures were observed, and the relatively homogeneous mixture maintained the pollution within the layer under 0.5 km. Ozone Monitoring Instrument (OMI) NO_2 products based on well-known DOAS trace gas fitting algorithm and WRF-Chem model further illustrated the simultaneous enhancement of NO_2 during the observation period. Backward trajectories suggest that long-range pollution transportation from northwest China contributes more to this pollution event.
© 2016 Published by Elsevier B.V.

1. Introduction

Atmospheric aerosol that comprises liquid and solid particles dispersed in the atmosphere can directly affect the earth's radiation budget

* Corresponding author at: School of Earth and Space Sciences, University of Science and Technology of China, Hefei 230026, China.
E-mail address: chliu81@ustc.edu.cn (C. Liu).

http://dx.doi.org/10.1016/j.scitotenv.2016.09.189
0048-9697/© 2016 Published by Elsevier B.V.

by scattering and absorbing solar and terrestrial radiation and indirectly by disturbing clouds, acting as cloud condensation nuclei (CCN) and ice nuclei (IN) (Charlson et al., 1991, 1992; Ramanathan and Feng, 2009; Haywood and Boucher, 2000). Aerosol particles are ubiquitous in Earth's atmosphere. They influence the quality of life in many ways—for example, through their climatic and health effects by affecting visibility. Moreover, many observational lines of evidence have shown that aerosols may have an unexpected influence on global climate, regardless of the relative importance of natural versus anthropogenic causes. Thus, it is important for us to understand aerosol properties. It is difficult to distinguish anthropogenic from natural aerosols and identify the exact pollution source because precise description of aerosol composition requires in situ chemical measurements that are restricted in time and location. However, it is possible to estimate the related pollution contributor using a combination of remote sensing, satellite data and information on urban and agricultural activities.

Beijing, located in North China, is one of the most populated and polluted regions in the country and has suffered severe air pollution problems in recent years, such as high concentration of particulate matter and poor visibility, resulting in adverse effects on people's lives. Thus far, several extensive studies using different methods have been conducted in North China, with particular focus on aerosol pollution. For example, Tesche et al. (2007) presented lidar observations of particle optical properties (backscatter coefficient, extinction coefficient and lidar ratio) in Beijing. Xue et al. (2010) reported the results of the measurements of sulfur dioxide (SO_2) and aerosol scattering coefficient obtained from several aircraft campaigns in summer and autumn of 2007 in the northeastern regions of China. Pan et al. (2013) measured trace elements of size-resolved aerosols at a rural site in North China, and found that the metallic episodes were attributable to long-range transportation. Zhu et al. (2014) investigated the temporal aerosol optical property over the regional background atmosphere of North China based on AERONET level 2.0 data. Guo et al. (2014) illustrated the similarity and difference in particulate matter formation between Beijing and other regions in other parts of the world. Recently, Sun et al. (2016) conducted aerosol particle measurements on a meteorological tower in urban Beijing to investigate the variations in particulate composition, sources and size distributions in response to emission controls during the 2014 Asia-Pacific Economic Cooperation (APEC) summit. However, knowledge on the synchronous optical properties of aerosol particles and NO_2 over northern China is particularly sparse, at least in the vertical scale. Therefore, experimental and high-precision data in

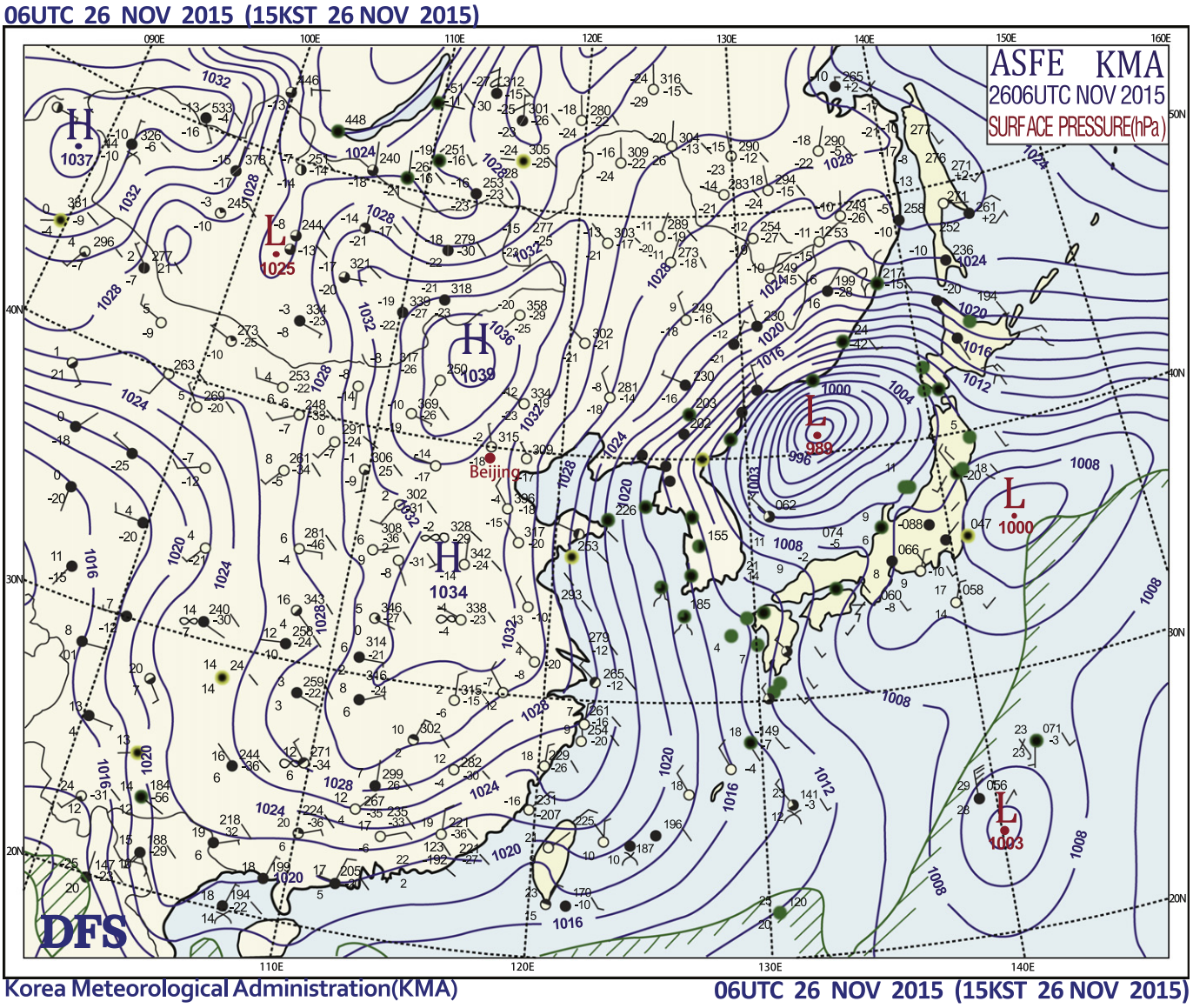

Fig. 1. Synoptic image of Beijing on November 26, 2015 by Korea Meteorological Administration.

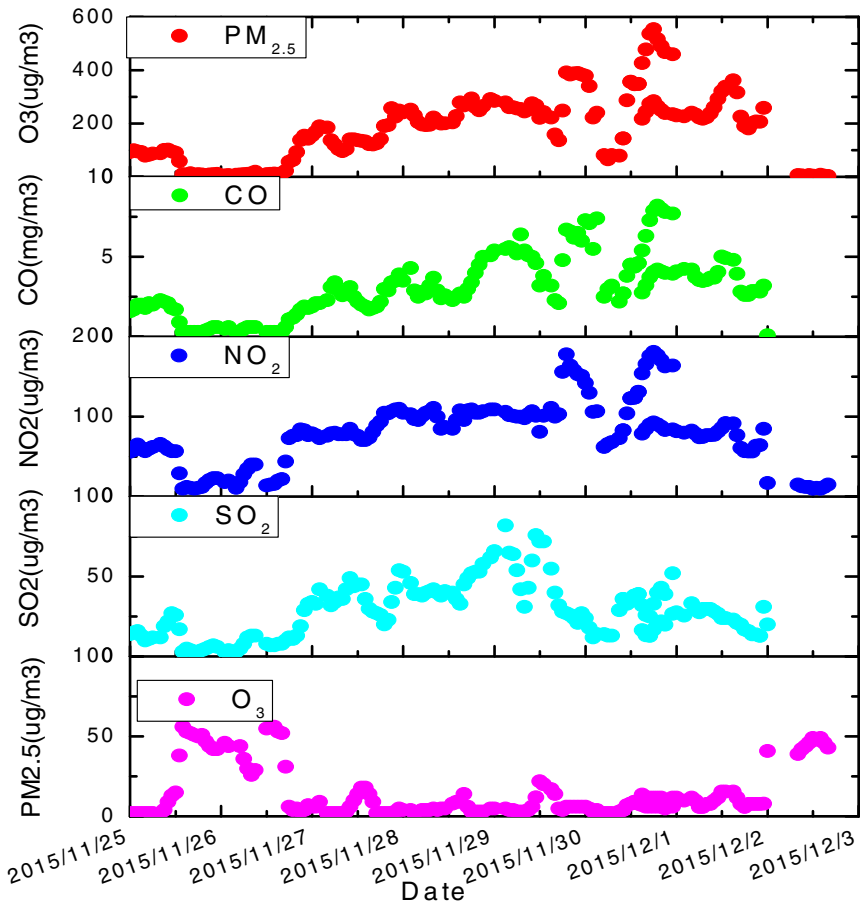

Fig. 2. Hourly variations of $PM_{2.5}$ concentration (red line), CO (green line), NO_2 (blue line), SO_2 (cyan line) and O_3 concentration (magenta line) from November 25 to December 3, 2015.

northern China are urgently needed to assess the role of aerosols in scenarios of pollution transportation and the impact on global changes.

The main objective of this paper is to investigate the optical properties of atmospheric aerosols and nitrogen dioxide (NO_2) in Beijing in winter 2015. In this integrative campaign, we implemented a series of remote sensing instruments such as a 532-nm Mie backscattered lidar, and a MAX-DOAS in combination with information from in situ measurements, to study transport processes. The methodologies discussed include analyzing aerosol and trace gas observations together with satellite data and trajectory analysis. In this paper, aerosol, NO_2 and OMI NO_2 from November 25 to November 30 are discussed. Aerosol and NO_2 data have been processed using C++ from a 532-nm Mie backscattered lidar and a MAX-DOAS, which are both developed by Anhui Institute of Optics and Fine Mechanics, Chinese Academy of

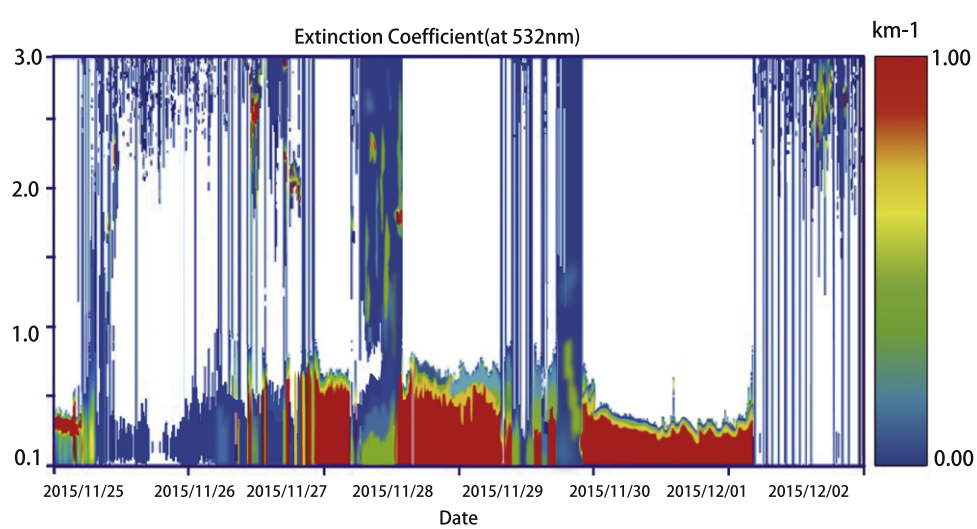

Fig. 3. Time sequence plots of aerosol measured by lidar at 532 nm from November 25 to December 2, 2015 (linear axes for both x-axis and y-axis).

ciences (AIOFM, CAS). The meteorological information is collected from the Korea Meteorological Administration, and the in situ measurements of $PM_{2.5}$, NO_2, carbon oxide (CO), sulfur dioxide (SO_2), and ozone (O_3) are taken from the China Ministry of Environmental Protection. The NOAA/ARL (National Oceanic and Atmospheric Administration/Air Resources Laboratory) Hybrid Single-Particle Lagrangian Integrated Trajectory (HYSPLIT) model was used to calculate the backward trajectories of air masses during our observation period (Draxler and Rolph, 2003).

2. Experimental methods

2.1. Experiment

Beijing, which is located in North China, is heavily affected by air pollution. A number of factors contribute to the high pollutant levels in the city. The most important of these factors is overpopulation (over 17 million), specifically pollution produced by human activities. Another important factor contributing to high levels of air pollution is specific topography. Beijing is surrounded by the Yanshan Mountains on the west, north and east, which makes the pollutants difficult to transport. This leads to the formation of strong inversions at night and a well-mixed convective boundary layer. From November to the beginning of December, integrated aerosol, NO_2 and in situ measurements were carried out at the Institute of Atmospheric Physics (IAP) between the north 3rd and 4th ring road in Beijing, which is a typical urban site surrounded mainly by residential areas. In this study, local time (LT) is used hereafter; note that it is 8 h ahead of the Coordinated Universal Time (UTC).

2.2. Instruments

2.2.1. 532-nm Mie lidar

The 532-nm Mie backscattered lidar is made up of three subsystems—emitting system, receiving system and signal analogue system. The laser source used is a pulsed Nd: YAG laser emitting short pulses at 532 nm. The pulse repetition rate is typically 20 Hz. The pulse duration is of the order of 6–9 ns. The light beam is expanded by a factor of 4, which reduces the divergence of the expanded beam to 2 mrad. The receiving telescope of the lidar system is based on a Cassegrainian design. The backscattered signals are then collected and focused on the telescope's focal point. Different interference filters suited to each wavelength are chosen to select the lidar wavelengths and to reject the atmospheric background radiation during daytime and nighttime operations. After separating and passing the respective interference filters, the photons elastically backscattered at the 532-nm wavelengths are detected with photo-multiplier tubes. With the 20-MHz sampling rate of the Licel transient recorder, the spatial resolution of 7 m can be attained. The control over the transient recorder and the preliminary and final treatment of the data is performed by LabView programs on a PC. After data pre-processing, the particle backscatter coefficient and the particle extinction coefficient at 532 nm could be retrieved using the Klett method (Klett, 1981).

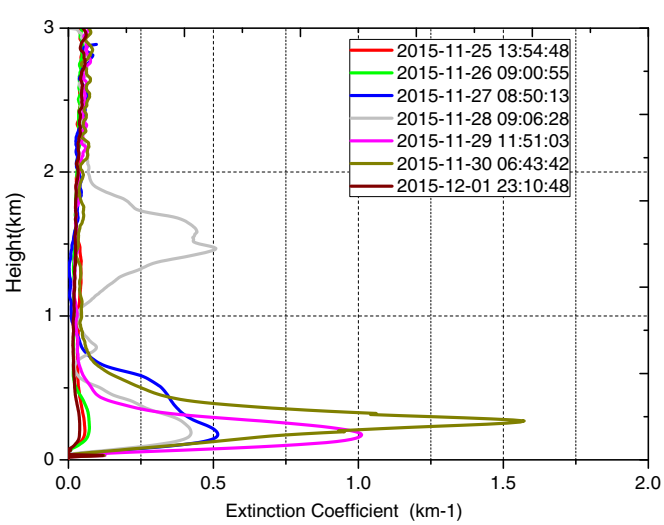

Fig. 4. Aerosol extinction profiles measured by lidar at 532 nm from November 25 to December 1, 2015.

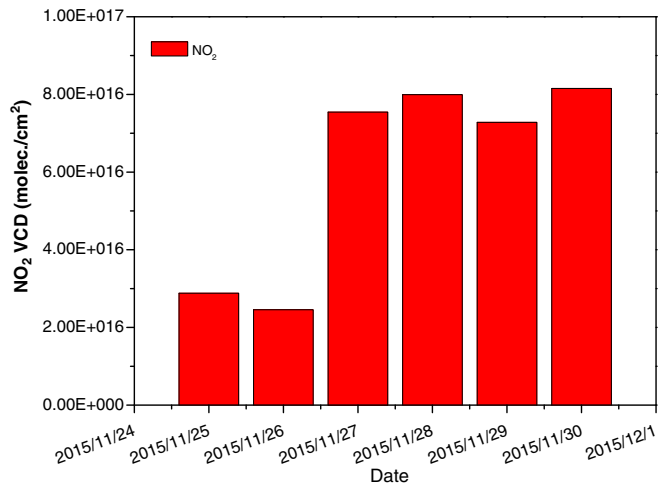

Fig. 5. Average value of NO_2 column density by MAX-DOAS from November 25 to November 30, 2015.

2.2.2. MAX-DOAS

MAX-DOAS is a special type of DOAS technology, which uses characteristic absorption structure of trace gases (such as NO_2, SO_2) in the visible ultraviolet band for the qualitative and quantitative analyses of gas. As a real-time and online measuring method, it is eminently suitable for remote sensing measurement of air pollution. Moreover, the data on the vertical column density of pollution gases can help in verifying satellite results (Krijger et al., 2007; Wagner et al., 2007; Irie et al., 2008; Schönhardt et al., 2015; Pope et al., 2015). MAX-DOAS receives scattered sunlight from telescopes at different elevations. Based on the characteristic absorption spectrum of pollution gas, it inverses the

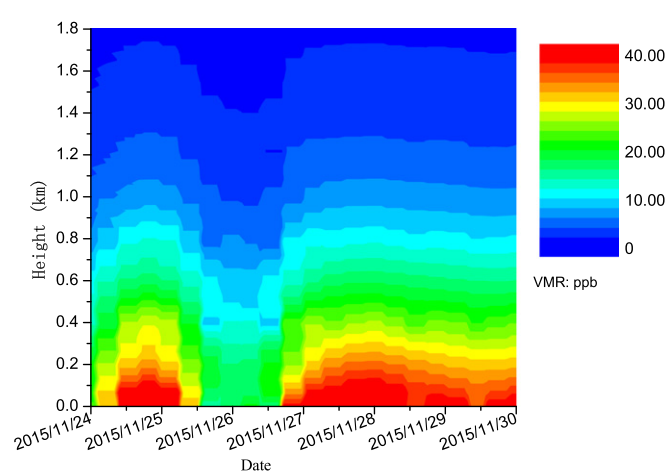

Fig. 6. NO_2 vertical profiles from November 25 to November 30, 2015.

vertical column density of pollution gas and distribution profile of density. Furthermore, it acquires data on the spatial distribution of pollution gas in the atmosphere by measuring the atmospheric absorption spectrum in zenith direction and several off-axis directions. During the monitoring process, the reflector orients itself to true north and is then driven by the stepper motor to turn to 1°, 2°, 3°, 4°, ..., 90° to finish one measurement cycle, thus realizing measurement of different angles.

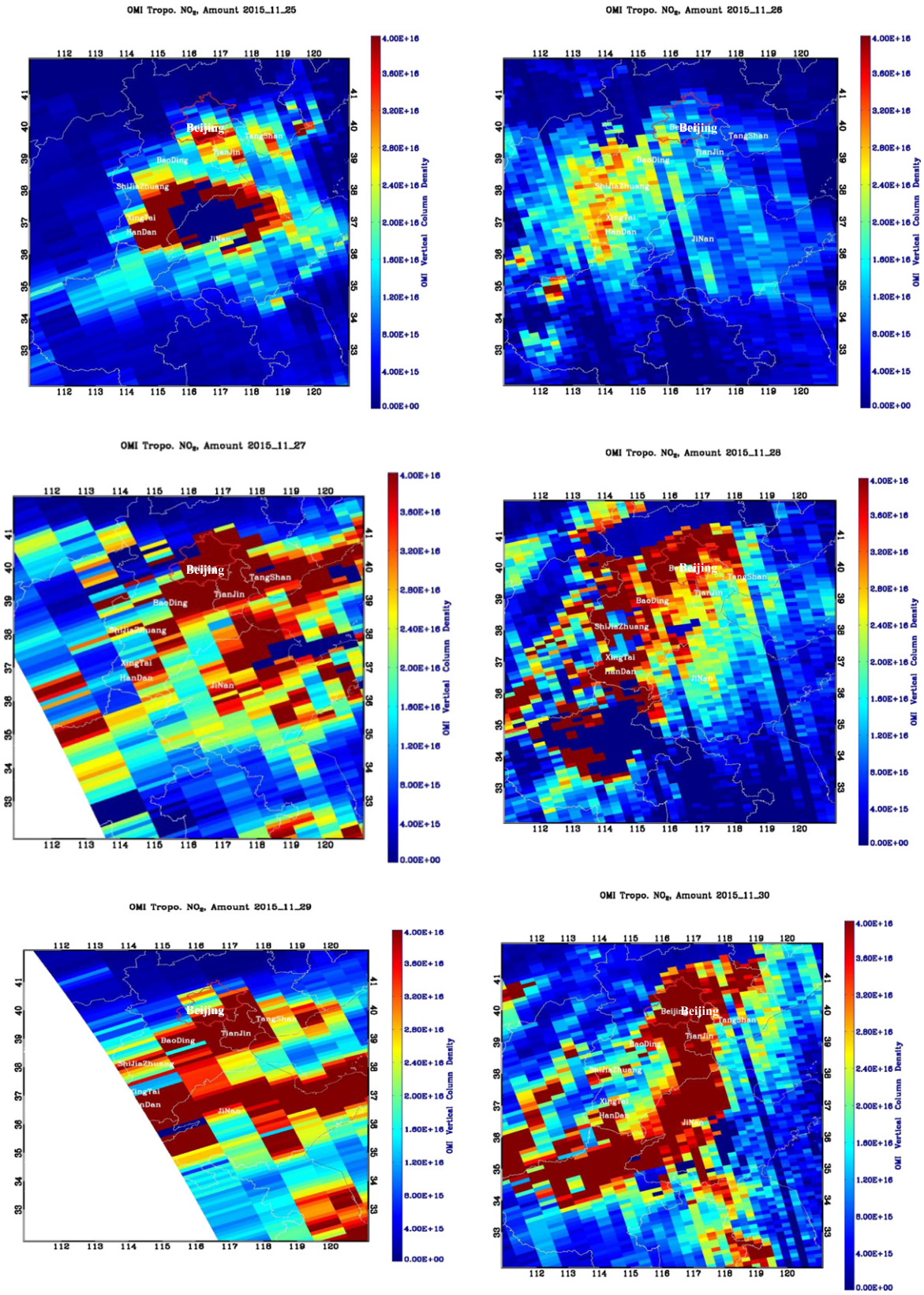

Fig. 7. Daily mean tropospheric NO_2 column from November 25 to November 30 (Fig. 7(a)–Fig. 7(f)), 2015 from OMI for mostly clear conditions (cloud radiance fraction <50%).

3. Data analysis

3.1. Meteorological condition

Meteorological data extracted from the daily weather maps and automatic meteorological stations of the Korea Meteorological Administration were used for analysis. This air stagnation condition prevailed from November 25 to November 30. During this pollution period, the surface high-pressure system was centered over Beijing and elongated to northeastern China. On November 26, a westerly trough and cold front were the prevailing synoptic systems at high altitudes (Fig. 1). The Asian continent was dominated by the northwesterly wind behind the trough, with intensive isobars associated with strong winds. At sea level, a low pressure area occurred in the Sea of Japan, with a large cold high entrenched over the west of Baikal Lake, Mongolia, and northern China. Beijing is located in the northwestern edge of the surface high pressure and influenced by the frequently changing winds between moderate northerly and southerly winds. During our transition and pollution periods, the wind shifted from northerly to southerly with decreasing speed, bringing air masses from the more populated southern industrial regions. And the winds in the boundary layer during the daytime were weak, generally <2 m/s. As for the geographic position, Beijing is a transition zone of the East Asian monsoon system, where different air masses meet under the control of large-scale monsoon winds. Such monsoon flows put Beijing as a receptor of the large amounts of pollutant emissions in the East Asian Pacific Rim (EAPR). Furthermore, the Horseshoe terrain enables the long-range transported pollutants from the southern regions to be detained in Beijing.

3.2. In situ measurements

The observed average hourly variations of $PM_{2.5}$, CO, NO_2, SO_2 and O_3 from November 25 to November 30 are shown in Fig. 2. During this period, a particulate pollution event broke out in Beijing. The event started on November 26 and ended on December 2 (1 week), during which RH values were generally <80%. Throughout the event, the measured concentrations of pollutants in the study area varied as a function of time, while peaks in SO_2, NO_2, CO and $PM_{2.5}$ all occurred in succession during the daytime. Specifically, $PM_{2.5}$ concentrations increased from 60 μg/m^3 and remained elevated until December 2. $PM_{2.5}$ concentrations reached their highest value at 1800 LT on November 30 (555 μg/m^3), and simultaneously large SO_2 and NO_2 enhancements were also observed a bit earlier with peak values corresponding to 76 μg/m^3 at 1100 LT on November 29 (SO_2), 181 μg/m^3 at 0600 LT on November 30 (NO_2), and 7.3 mg/m^3 at 1200 LT on November 30 (CO), respectively. There was a significant time lag of one day between peak concentration of particles and precursors, indicating possible photochemical processes and effects on the pollutants. In addition, NO_2 and SO_2 did not follow a classical diurnal cycle near the surface, and their mean levels in the pollution event were higher than their seasonal means. However, the diurnal cycle of ground-level O_3 concentration showed a mid-day peak and lower nighttime concentrations, and exhibited an overall negative relationship with precursors and particles. It is reasonable that any increase in the level of NO_2 is invariably accompanied by a reduction in the level of O_3, although the levels of O_3 and NO_2 are inextricably linked owing to the chemical coupling of O_3 and NO_x. Moreover, changes in the local level of O_3 and NO_2 will lead to an increasing background level.

3.3. Aerosols by lidar

The aerosol extinction profiles derived from lidar at a high temporal resolution reflects the vertical distribution and temporal variation of atmospheric aerosol. The real-time display of processed aerosol extinction from November 25 to December 2 is performed on a time available basis in Fig. 3. The aerosol measurements were taken at 532 nm at altitudes higher than 7 km during nighttime and up to 5 km above ground level

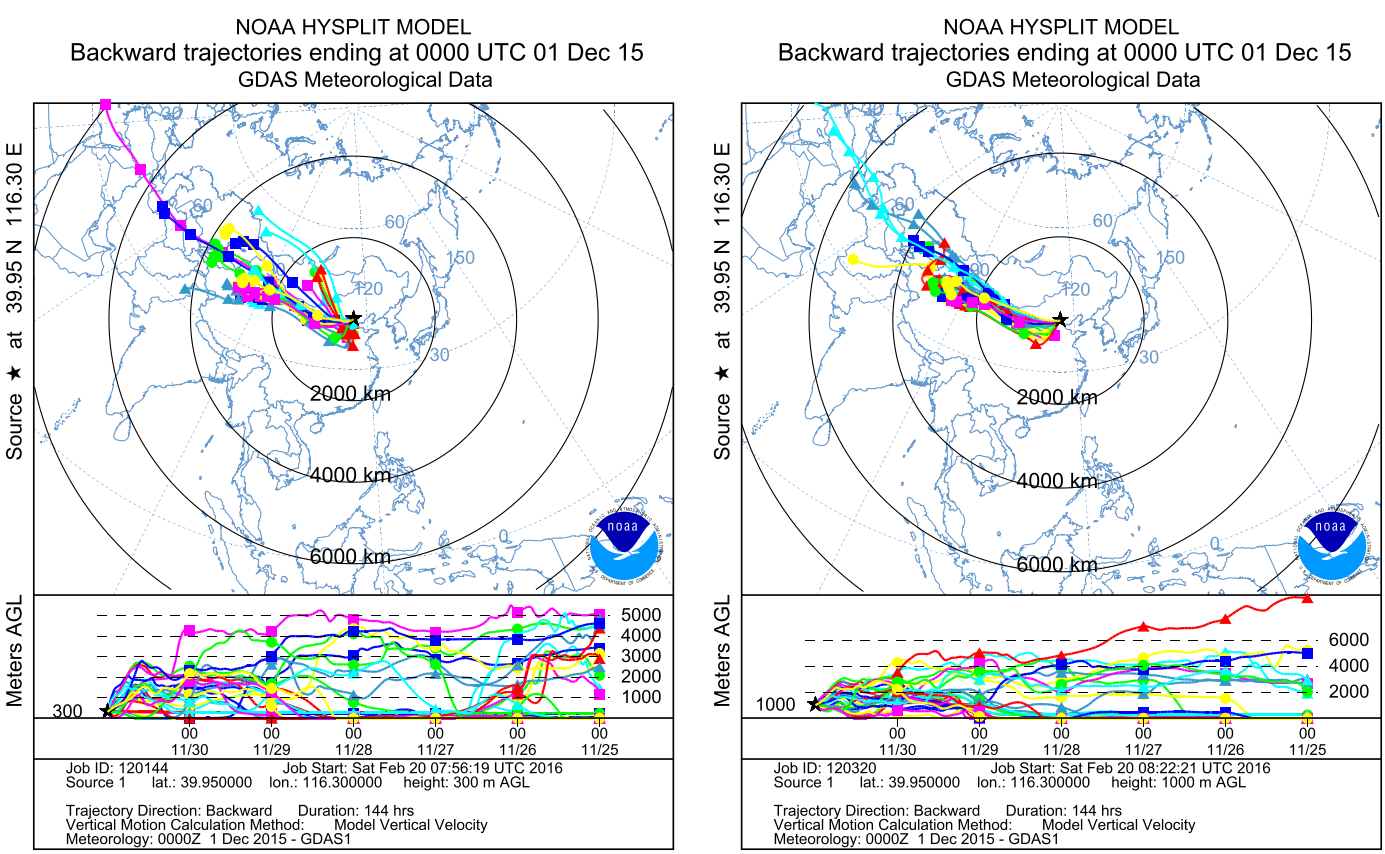

Fig. 8. Backward trajectories from HYSPLIT ensembles at 0.3 km (Fig. 8(a)) and 1.0 km (Fig. 8(b)) ending at Beijing, North China, at 00:00 UTC on December 1, 2015.

(AGL) during daytime. The measurements show a steady increase in the daily values of aerosol extinction concentrations, reaching 1.55 km^{-1} at 0.27 km on November 30 (Fig. 4). Wind shift and high surface pressure that eventually dissipated were the reason for the end of the time series and for the lower aerosol concentrations (compared to previous days). The high and almost stable extinction coefficients at altitudes lower than 0.5 km from November 27 to December 2 indicate a well-mixed boundary layer. Aerosol measurements, together with NO_2 observations (see Section 3.4) from MAX-DOAS, suggest that the height of the mixing layer in the early afternoon is between 0.2 and 0.5 km. During the last two days, a detachment of the top of the pollution layer is clearly seen in Fig. 4. From selected aerosol extinction vertical profiles in Fig. 4, the aerosol extinction coefficient increased with altitude from the ground to 0.2 km, and the daily averaged extinction value from 0.1 km to 3 km on November 25 was 0.019 km^{-1}. At 0900 LT on November 26, the initial stage of the event, the aerosol extinction profile increased slightly with altitude and peaked at 0.21 km (0.072 km^{-1}), but subsequently decreased and reached a minimum at 2 km (0.006 km^{-1}). Then, in the mid-stage of the pollution, the aerosol extinction profiles increased dramatically and peaked at 0.515 km^{-1} at 0850 LT on November 27 and 0.43 km^{-1} at 0906 LT on November 28 at a height of 0.225 km. In the next two days, the average value of extinction coefficients continued to increase and soared to 1.0 km^{-1} at 1151 LT on November 29 at a height of 0.195 km and 1.55 km^{-1} on November 30 at a height of 0.27 km, respectively. In the later stage, aerosol extinction profiles on December 1 dipped substantially, and the maximum value was much lower at 0.39 km^{-1} at approximately 0.235 km. After the event, the aerosol extinction profile maintained a downward trend and reduced to a level that was similar to that of a clear day before the pollution period at 0.028 km^{-1}. The relatively higher aerosol extinction profile distributed within the boundary layer implied that most particulate pollutants accumulated in the surface atmosphere. Hence, it is reasonable that the aerosols in the lower atmospheric layers were transported primarily from remote dust sources in northern China.

3.4. Surface NO_2 observations by MAX-DOAS

The atmospheric lifetime of NO_x against oxidation is of the order of hours (Atkinson, 2000; Zatko et al., 2013), resulting in large spatial and temporal variability around source areas. High concentrations are mainly restricted to the boundary layer up to 1–2 km, with rapid drop-off at higher altitudes. Fig. 5 shows average NO_2 columns measured at the locations of IAP stations from LT 1000 and LT 1600 under cloud-free conditions during the observation period. The results showed that NO_2 experienced an upward trend from November 25 despite a slight decrease on November 26. The column density stood at $2.8815E * 10^7$ and reached maximum at $8.1528E * 10^7$ on November 30, which is coincidental with aerosol evolution. The height of the NO_2 layer was concentrated below 0.3 km and was elevated from 0.2 km on November 27 to 0.3 km on November 28 in Fig. 6. Then, the NO_2 layer evolved slightly and was maintained at a height of 0.3 km. The higher NO_2 can be explained by daytime photochemical loss of NO, dampened by the diurnal cycle of anthropogenic NO_x emissions that has a broad daytime maximum. Compared to the in situ measurements of NO_2 in Fig. 2, the diurnal variation of tropospheric NO_2 columns showed insignificant diurnal cycle and suggested that NO_2 concentration in this event was more influenced by background air pollution, specific emission conditions and general meteorological conditions.

3.5. Satellite NO_2 observations

OMI on board NASA's EOS-Aura satellite (launched in July 2004) provides tropospheric NO_2 columns and valuable information on the distribution of NO_2 in Beijing and its adjacent areas. OMI observes the Earth's atmosphere continuously in nadir mode with a 114 field-of-view (2600 km on the Earth's surface), thereby achieving daily global coverage (Konovalov et al., 2006; Boersma et al., 2008, 2009; Curier et al., 2014). The small-pixel OMI observations used here are representative for the urban scale and are more likely to show the local weekend emission reductions. Furthermore, the nadir spatial resolution of 13×24 km^2 allows for the observation of finer details, and increases the likelihood of encountering cloud-free scenes. In this study, OMI tropospheric NO_2 product from Univeristy of Science and Techology of China (USTC) are used. More specifically, tropospheric NO_2 Slant Column Density (SCD) are retrieved by the DOAS trace gas fitting algorithm using a nonlinear least-squares (NLLS) inversion technique from the OMI spectra. Accounting for local atmospheric conditions, WRF-Chem model with measured climatology parameter and newest emission inventory is then used to simulate trace gas profiles for NO_2 Vertical Column Density (VCD) products conversion from former calculated SCD (Liu et al., 2016). The acquisition of regional density distribution data is significant for the investigation of the processes of generation and transportation of pollution. To evaluate this apparent seasonal cycle in the diurnal cycle, we compared NO_2 at 10:00 and 13:45 observed from satellites and surface stations. We do not require spatial or temporal coincidence between satellite and surface measurements; we only require that both techniques perform measurements under mostly clear conditions. As indicated in Fig. 7, OMI retrievals also reveal much greater NO_2 over Beijing and its adjacent areas during this pollution event. This makes it clear that NO_2 loading over Beijing peaked on November 30, and has since shown an overall increasing trend despite the low NO_2 concentration on November 26. The reduction on November 26 may reflect a temporary diffusion, but it is followed by a rapid resurgence of transported pollution in the following days.

4. Sources

Examining the location from which air masses originate can provide insights into potentially pollution sources located upwind of the receptor site. This can be accomplished using air mass back-trajectories, which have been used in the past to link atmospheric concentrations to pollution sources (Larissi et al., 2010; Rozwadowska et al., 2010). In this study, back-trajectories were calculated using the Hybrid Single-Particle Lagrangian Integrated Trajectory (HYSPLIT-4) model. In this analysis, 144-h back-trajectories were calculated for air masses arriving at heights of 0.3 km and 1.0 km above ground level at our observation sites. During the pollution period (Fig. 8), the air masses, whether below 0.3 km or below 1.0 km, were homogeneously long-range pollution transportation from the northwestern portion of China. This particular region is more characterized as large areas of land with little or no vegetation, and more dust can be transported through the upwind side of the mountains by westerly and large-mountain breezes moving toward cities. Furthermore, the burning of fossil fuels used in vehicles, power plants and various industrial processes can also contribute in increased concentrations.

5. Conclusions

Ground-based remote sensing can sample the lowest part of the atmosphere, where most of the aerosols and NO_2 reside and strong gradients exist. Our observation focused on urban locations in Beijing during winter in 2015. The obtained aerosol backscatter profiles indicate the arrival of pollution layers transported from distant sources together with the simultaneously increased aerosols and NO_2 concentrations, as well as the increased concentrations of other precursors. The secondary contaminants, ozone and a large percentage of NO_2 did not show the usually clear diurnal cycle in this event, indicating that the shape and amplitude of their cycles are strongly influenced by meteorological conditions and prevailing levels of background precursors. Moreover in situ measurements of NO_2 concentrations also show a significant correlation with collocated OMI tropospheric NO_2 column retrievals. We conclude that combined observations of particles and NO_2 backed by

measurements of anthropogenic trace gases (CO, SO_2, O_3) form unique tracers to detect pollution layers in the atmosphere. Furthermore, sources of enhanced particle concentrations and NO_2 are more likely from long-range transport of dust, burning of fossil fuels from power plants and various industrial processes from anthropogenic emissions.

Author contributions

All authors contributed measurements and/or analysis for this manuscript. Specifically, Wenqing Liu designed the field campaign and Zhenyi Chen carried out the analytical procedures. Cheng Liu performed satellite observations. Tianshu Zhang provided valuable comments to improve the manuscript. Zhenyi Chen prepared the manuscript with contributions from all co-authors.

Acknowledgments

This work is supported by the project, Key Project of Chinese National Programs for Fundamental Research and Development (973 Program) (2014CB447900) and National Natural Science Foundation of China (41305126, 41575021, 91544212). The field activities would not have been possible without the experimental site provided by the Institute of Atmospheric Physics (IAP), facilitated by Zifa Wang and Yele Sun, who are greatly thanked. The authors also gratefully acknowledge the NOAA Air Resources Laboratory (ARL) for providing the HYSPLIT transport and dispersion model used in this research.

References

Atkinson, R., 2000. Atmospheric chemistry of VOCs and NOx. Atmos. Environ. 34 (12–14), 063–2101.

Boersma, K.F., Jacob, D.J., Eskes, H.J., Pinder, R.W., Wang, J., van der A, R.J., 2008. Intercomparison of SCIAMACHY and OMI tropospheric NO_2 columns: observing the diurnal evolution of chemistry and emissions from space. J. Geophys. Res. 113, D16.

Boersma, K.F., Jacob, D.J., Trainic, M., Rudich, Y., DeSmedt, I., Dirksen, R., Eskes, H.J., 2009. Validation of urban NO_2 concentrations and their diurnal and seasonal variations observed from space (SCIAMACHY and OMI sensors) using in situ measurements in Israeli cities. Atmos. Chem. Phys. 9, 867–3879.

Charlson, R.J., Langer, J., Rodhe, H., Leovy, C.B., Warren, S.G., 1991. Perturbation of the Northern Hemisphere radiative balance by backscattering form anthropogeniec sulfate aerosols. Tellus 43, 152–163.

Charlson, R.J., Schwartz, S.E., Hales, J.M., Cess, R.D., Coakley Jr., J.A., Hansen, J.E., Hofmann, J.D., 1992. Cliamate forcing by anthropogenic aerosols. Science 225, 423–430.

Curier, R.L., Kranenburg, R., Segers, A.J.S., Timmermans, R.M.A., Schaap, M., 2014. Synergistic use of OMI NO_2 tropospheric columns and LOTOS-EUROS to evaluate the NOx emission trends across Europe. Remote Sens. Environ. 149, 58–69.

Draxler, R.R., Rolph, G.D., 2003. HYSPLIT (Hybrid Single-Particle Lagrangian Integrated Trajectory) model (access via NOAA ARL READY web site (http://www.arl.noaa.gov/ready/hysplit4.html)) NOAA Air Resources Laboratory, Silver Spring, MD.

Guo, S., Hu, M., Zamora, M.L., Peng, J.F., Shang, D.J., Zheng, J., Du, Z.F., Wu, Z.J., Shao, M., Zeng, L.M., Molina, M.J., Zhang, R.Y., 2014. Elucidating severe urban haze formation in China. PNAS 111, 17373–17378.

Haywood, J., Boucher, O., 2000. Estimate of the direct and indirect radiative forcing due to tropospherci aerosols: a review. Rev. Geophys. 38, 513–543.

Irie, H., Kanaya, Y., Akimoto, H., Tanimoto, H., Wang, Z., Gleason, F.J., Bucsela, E.J., 2008. Validation of OMI tropospheric NO_2 column data using MAX-DOAS measurements deep inside the North China Plain in June 2006. Atmos. Chem. Phys. Discuss. 8, 8243–8271.

Klett, J.D., 1981. Stable analytical solution for processing lidar returns. Appl. Opt. 20, 211–220.

Konovalov, I.B., Beekmann, M., Richter, A., Burrows, J.P., 2006. Inverse modelling of the spatial distribution of NOx emissions on a continental scale using satellite data. Atmos. Chem. Phys. 206, 1747–1770.

Krijger, J.M., van Weele, M., Aben, I., Frey, R., 2007. Technical note: the effect of sensor resolution on the number of cloud-free observations from space. Atmos. Chem. Phys. 7, 2881–2891.

Larissi, I.K., Koukouletsos, K.V., Moustris, K.P., Antoniou, A., Paliatsos, A.G., 2010. PM10 concentration levels in the greater Athens area, Greece. Fresenius Environ. Bull. 19, 226–231.

Liu, H.R., Liu, C., Xie, Z.Q., Li, Y., Huang, X., Wang, S.S., Xu, J., Xie, P.H., 2016. A paradox for air pollution controlling in China revealed by "APEC Blue" and "Parade Blue". Sci. Rep. 6, 34408.

Pan, Y.P., Wang, Y.S., Sun, Y., Tian, S.L., Cheng, M.T., 2013. Size-resolved aerosol trace elements at a rural mountainous site in Northern China: importance of regional transport. Sci. Total Environ. 461, 761–771.

Pope, R.J., Chipperfield, M.P., Savage, N.H., Ordóñez, C., Neal, L.S., Lee, L.A., Dhomse, S.S., Richards, N.A.D., Keslake, T.D., 2015. Evaluation of a regional air quality model using satellite column NO_2: treatment of obsertvation errors and model boundary conditions and emissions. Atmos. Chem. Phys. 15, 5611–5626.

Ramanathan, V., Feng, Y., 2009. Air pollution, greenhouse gases and climate change: global and regional perspectives. Atmos. Environ. 43, 37–50.

Rozwadowska, A., Zielinski, T., Petelski, T., Sobolewski, P., 2010. Cluster analysis of the impact of air back-trajectories on aerosol optical properties at Hornsund, Spitsbergen. Atmos. Chem. Phys. 10, 877–893.

Schönhardt, A., Altube, P., Gerilowski, K., Krautwurst, S., Hartmann, J., Meier, A.C., Richter, A., Burrows, J.P., 2015. A wide field-of-view imaging DOAS instrument for two-dimensional trace gas mapping from aircraft. Atmos. Meas. Tech. 8, 5113–5131.

Sun, Y.L., Wang, Z.F., Wild, O., Xu, W.Q., Chen, C., Fu, P.Q., Du, W., Zhou, L.B., et al., 2016. "APEC blue": secondary aerosol reductions from emission controls in Beijing. Sci. Rep. 6, 20668.

Tesche, M., Ansmann, A., Müller, D., Althausen, D., Engelman, R., 2007. Particle backscatter, extinction, and lidar ratio profiling with Raman lidar in south and north China. Appl. Opt. 46, 6302–6308.

Wagner, T., Ibrahim, O., Sinreich, R., Frieß, U., von Glasow, R., Platt, U., 2007. Enhanced tropospheric BrO over Antarctic sea ice in mid winter observed by MAX-DOAS on board the research vessel Polarstern. Atmos. Chem. Phys. 7, 3129–3142.

Xue, L.K., Ding, A.J., Gao, J., Wang, T., Wang, W.X., Wang, X.Z., Lei, H.C., Jin, D.J., Qi, Y.B., 2010. Aircraft measurements of the vertical distribution of sulfur dioxide and aerosol scattering coefficient in China. Atmos. Environ. 44, 278–282.

Zatko, M.C., Grenfell, T.C., Alexander, B., Doherty, S.J., 2013. The influence of snow grain size and impurities on the vertical profiles of actinic flux and associated NOx emissions on the Antarctic and Greenland ice sheets. Atmos. Chem. Phys. 13, 3547–3567.

Zhu, J., Che, H.Z., Xia, X.G., Chen, H.B., P., G., Zhang, W.X., 2014. Column-integrated aerosol optical and physical properties at a regional background atmosphere in North China Plain. Atmos. Environ. 84, 54–64.